ARTICLE

Low-Bias Conductance Mechanism of Diarylethene Isomers: a First-principle Study

Ming-lang Wang*, Guang-ping, Zhang, Xiao-xiao Fu, Chuan-Kui Wang*

School of Physics and Electronics, Shandong Normal University, Jinan 250358, China

(Dated: Received on November 14, 2019; Accepted on March 27, 2020)

The structure-property relationship of diarylethene (DAE)-derivative molecular isomers, which involve ring-closed and ring-open forms, is investigated by employing the non-equilibrium Green's function formalism combined with density functional theory. Molecular junctions are formed by the isomers connecting to Au(111) electrodes through flanked pyridine groups. The difference in electronic structures caused by different geometry structures for the two isomers, particularly the interatomic alternative single bond and double bond of the ring-closed molecule, contributes to the vastly different low-bias conductance values. The lowest unoccupied molecular orbital (LUMO) of the isomers is the main channel for electron transport. In addition, more electrons transferred to the ring-closed molecular junction in the equilibrium condition, thereby decreasing the LUMO energy to near the Fermi energy, which may contribute to a larger conductance value at the Fermi level. Our findings are helpful for understanding the mechanism of low-bias conductance and are conducive to the design of high-performance molecular switching based on DAE or DAE-derivative molecules.

Key words: Molecular electronics, Molecular switching, Density functional theory, Non-equilibrium Green's function

I. INTRODUCTION

The core task in single-molecule electronics is to establish a relationship between molecular structures and their transport properties [1–8] and utilizing that to achieve functional electronic devices, such as sensors [9–13], memories [14–17], light-emitting diodes or transistors [18–23], field-effect transistors [24–27], and negative differential resistance devices [28–30]. A highly challenging and promising aspect is to create molecular switching, which has two isomeric states since the seminal work was reported by Jia *et al.* [31–34]. The isomeric states can be tuned or interchanged through external stimuli, such as electrons [35–37], electric fields [38, 39], and light irradiation [31, 40–43]. To achieve applicable molecular switching, isomeric states must be preserved at the molecular junction, which can result in a significantly high-low conductance ratio. Diarylethenes (DAEs), which have good thermal stability and high fatigue resistance, are a promising type of molecule to realize the abovementioned behavior because they can switch structures between ring-closed and ring-open forms [44–46]. The electronic structures or conjugation characteristics change significantly, resulting in vastly different conductance values and prominent high-low conductance ratios ranging from 10 to 300 [31, 47–50]. However, alternating the two conductance states continuously remains challenging. According to a large number of studies in recent years [31, 46, 50, 51, 62, 63], the electron transport properties of DAE depend on the anchoring group, electrode properties, and switch core sulfur atoms in the thiophene ring of DAEs. The sulfur atoms interact strongly with the metallic surface, which can affect the switching properties. Meanwhile, the interaction between electrodes and the core sulfur atoms may hinder the switching process. In addition, an appropriate interfacial interaction between electrodes and DAE molecules must occur to yield a large conductance; however, it does not change the molecular switching function. To obtain an ideal switch using a DAE molecule, the conductance mechanism of DAE molecular junctions must be understood. Recently, a DAE derivative functionalized with oxygen instead of sulfur in thiofuran to form furan has been synthesized to reduce interactions with metal substrates; in this case, using a scanning tunneling microscope probe is beneficial for investigating the electronic transport characteristics [48, 50, 51]. Although a good on-off ratio was observed in the experimental measurement, the characteristics of electron transport must be further elucidated.

In this study, we theoretically investigated the structure-property relationship of a DAE derivative (C5F-4Py) accessed on Au(111) electrodes by employing the non-equilibrium Green's function formalism

*Author to whom correspondence should be addressed. E-mail: wangminglang@sdnu.edu.cn, ckwang@sdnu.edu.cn

DOI:10.1063/1674-0068/cjcp1911204

combined with density functional theory (NEGF+DFT method) [52–56], while focusing on the internal transport mechanism of open-circle and close-circle isomers and the reason for the different conductance values. Our calculations show that the low-bias conductance is predominantly attributed to the lowest unoccupied molecular orbital (LUMO) of both DAE derivatives. When the structure of the DAE-derivative molecule changes from an open-circle to a closed-circle, an excellent conductive path is formed, which is similar to the single bond and double bond alternative alkene throughout the molecular backbone. This results in a more delocalized electron distribution and a more remarkable π-conjugation, which facilitate electron transfer. Additionally, more electrons are transferred to the closed-circle conformation in the equilibrium condition, which decreases the energy level of the LUMO to near to the Fermi energy. Consequently, an appropriate on-off ratio is obtained by interchanging the different conformations of the DAE-derivative molecules.

II. THEORETICAL AND COMPUTATIONAL DETAILS

The SIESTA software package was employed to investigate the geometric and electronic structures of molecular junctions, such as Au-molecule-Au. After capturing optimized junctions, the SMEAGOL code was used to study electronic transport properties [56, 57]. It is well known that SIESTA is an efficient DFT program that can numerically simulate large systems with affordable resources. The wave functions of valence electrons are expanded over a finite-range numerical basis set, and the core electrons are described by norm-conserving Troullier-Martins pseudopotentials [58, 59]. Whereas a double-zeta plus polarization (DZP) basis set was used for H, C, O, N, and F atoms, two different types of basis set functions were used for Au in the bulk and at the surface, respectively. More specifically, a DZP basis set extended with diffuse functions was used to describe Au surface atoms, and a single-zeta plus polarization basis set was used for the bulk. The exchange-correlation functional was treated at the level of generalized gradient approximation (GGA) formulated by the Perdew-Burke-Ernzerhof (PBE) [60]. The real-space grid was equivalent to a cutoff of 200.0 Ry. Geometry optimization was performed using the standard conjugate gradient method until all the atomic forces were smaller than 0.03 eV/Å.

SMEAGOL was employed to implement the NEGF+DFT approach, which utilizes SIESTA as the DFT platform [57]. Periodic boundary conditions were applied in the plane, which was transverse to the transport direction. The unit cell of the extended molecule included a central switching molecule and 10 atomic layers of Au electrodes with a (4×4) supercell. Furthermore, 24 energy points along the semi-circle and 24 points along the line in the complex plane were used to integrate the charge density, whereas 24 poles were used for the Fermi function (the electronic temperature was 300 K). The transmission spectrum $T(E)$ of the Au-molecule-Au junction was evaluated as follows:

$$T(E) = \frac{1}{\Omega_{\mathrm{2DBZ}}} \int_{\mathrm{2DBZ}} T\left(\vec{k}; E\right) \mathrm{d}\vec{k} \tag{1}$$

where Ω_{2DBZ} is the area of the two-dimensional Brillouin zone in the transverse direction (orthogonal to the transport direction). The transmission coefficient $T(\vec{k}; E)$ was obtained as follows:

$$T(\vec{k}; E) = \mathrm{Tr}[\Gamma_{\mathrm{L}} G_M^R \Gamma_{\mathrm{R}} G_M^{(R+)}] \tag{2}$$

where G_M^R is the retarded Green's function matrix of the extended molecule; $\Gamma_{\mathrm{L}}(\Gamma_{\mathrm{R}})$, which is called the broadening function matrix, is used to describe the interface interaction between the extended molecule and the left-hand (right-hand) side electrodes. We calculated the transmission coefficient samples of 4×4 k-points in the transverse Brillouin zone and one k-point in the transport direction.

III. RESULTS AND DISCUSSION

1,2-Bis(2-methyl-5-((Z)-(2-cyano-2-(pyridine-4-yl)vinyl)furan-3-yl) hexafluoro-cyclopentene (C5F-4Py-O) can be synthesized according to Kim *et al.* [48]. When illuminated by ultraviolet light or stimulated by a voltage pulse, the closed isomer (C5F-4Py-C) of C5F-4Py can be observed in experiments [48, 50, 51, 61]. To resolve the switching mechanism, we first investigated the atomic and electronic structures of these two isolated isomers. For the C5F-4Py-O isolated molecule, its optimized atomic structure is shown in FIG. 1(a). On both sides of the central fluorocyclopentane, all the C, H, O, and N atoms were nearly coplanar separately, whereas the two flanked molecular groups were nearly perpendicular to each other with a dihedral angle of 80.0°, which can be ascribed to the steric effect of methyl (-CH_3). Specifically, the methyl moiety linked to furan was coplanar with the furan or pyridine plane. Considering that the length of C atoms in both methyl groups was 3.68 Å, we inferred that the interaction between them was weak and hence produced an open-circle structure. By contrast, the methyl moiety was almost perpendicular to the plane of furan with a dihedral angle of 98° in the C5F-4Py-C isomer. Considering the weak steric repulsion, two C atoms in the two furans interacted with each other to form a C−C bond with a length of 1.52 Å. The closed-cycle isomer is shown in FIG. 1(b). Because the molecular structure changed, the structure of alternative single bonds and double bonds between C atoms, *e.g.*, for olefins, is through the entire molecule. Consequently, the delocalization of molecular orbitals increased

DOI:10.1063/1674-0068/cjcp1911204

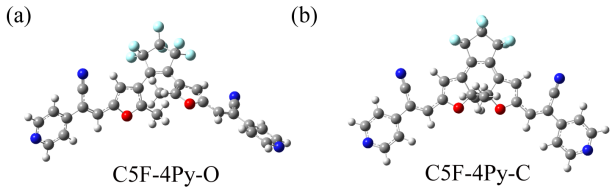

FIG. 1 Optimized atomic structures: closed-ring structure: C5F-4Py-O (a), open-ring structure: C5F-4Py-C (b).

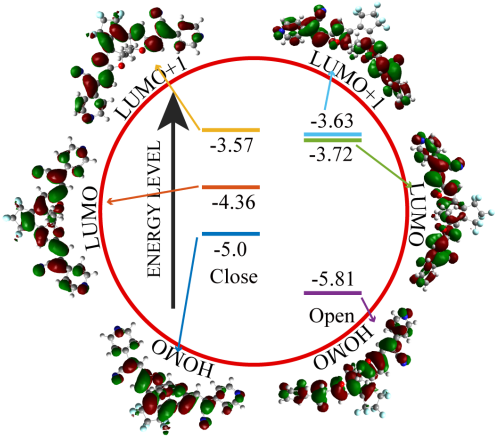

FIG. 2 Frontier molecular orbitals of isolated C5F-4Py isomers and their orbital energies.

and the conjugation of the molecule improved. To demonstrate these differences, the electronic structures were calculated and are shown in FIG. 2. Overall, all the frontier molecular orbitals exhibited excellent delocalization characteristics. In the case of the C5F-4Py-C molecule, the highest occupied molecular orbital (HOMO) and the LUMO were dominated by C 2p, N 2p, and O 2p atomic orbitals across the molecule. Nevertheless, the O 2p atomic orbital contributed by lone pair electrons was absent in LUMO+1. All of these orbitals contributed to the π-conjugation system, thereby enabling electron transfer along the entire molecule. Quantitatively, the energy gap between the HOMO and LUMO was 0.64 eV, which was less than the experimental value of 1.9 eV approximately [45]. This can be ascribed to the well-known deficiency of the exchange-correlation functional GGA-PBE. Because we only need to calculate the conductance ratio between the different isomers in this study, the difference in energy gap between the calculation results and experimental measurements can be disregarded and the system error can be cancelled. By contrast, the HOMO−LUMO gap was 2.1 eV in the case of C5F-4Py-O. Although this value was lower than the experimental value of 3.4 eV [45], the difference in energy gap between the two conformations was nearly identical. This further supports that the study based on the exchange-correlational GGA-PBE is acceptable. Furthermore, the HOMO energy of C5F-4Py-O was lower than that of C5F-4Py-C. The result can be verified by experimental observations [35, 37, 38]. The energy gap between the LUMO and LUMO+1 was only 0.09 eV, indicating that the two orbitals were degenerate. Their wave functions were similar, but a sign difference was observed in the left leg, as shown in FIG. 2. The O 2p atomic orbital appeared in the LUMO and LUMO+1, but it was absent in the HOMO. Considering the difference in electron density distribution between C5F-4Py-C and C5F-5Py-O, the conductance ratio must be calculated by connecting them to compose molecular junctions.

Next, we connected the C5F-4Py-C molecule to a protruding Au atom, which is called an adatom through flanked pyridines, to investigate its electronic transport properties. The optimized atomic conformation of the Au-C5F-4Py-C-Au molecular junction is shown in FIG. 3(a). We assumed that it was linked to the Au atom through the N atom in pyridine through the Au-N coordinate bond. The length of the Au−N bond was 2.19 Å, and the distance between the left and right electrodes was 20.53 Å, as defined by the distance between the adatoms in the transport direction. A comparison between the atomic structures of the isolated molecules with those in the molecular junction indicated the rigidity of the C5F-4Py-C molecule. This implies that its electronic structures can be maintained at the molecular junction. FIG. 3(b) shows the equilibrium transmission spectrum. It is clear that all the peaks in the transport spectrum are sharp, which verifies the weak interaction between the electrode and C5F-4Py-C molecule. In general, the transmission coefficient at the Fermi energy is dominated by its adjacent orbitals. Under the Fermi energy, the first transmission peak located at −0.44 eV decayed significantly toward the Fermi level (E_{F}), which did not contribute to the transmission coefficient. However, above the Fermi level, the transmission peak was close to the Fermi level with an energy separation of 0.02 eV. The other three prominent transmission peaks were located at −1.93, 0.85, and 1.88 eV, which contributed to three excellent conductive channels with high transmission coefficients. Considering their narrow widths, they were ascribed to weak interactions with the electrodes. The transmission coefficient calculated at the Fermi level was 2.5×10^{-1} G_0. Considering the weak interaction of the Au−N dative bond, we projected the transmission spectrum onto the frontier molecular orbitals of the central C5F-4Py-C molecule, as shown in FIG. 3(c). It is clear that the transmission peak at −0.44 eV was dominated by the HOMO and that at 0.85 eV was primarily from the LUMO+1. By contrast, the transmission peaks at 0.02 eV and the Fermi level were both dominated by the LUMO of the C5F-4Py-C molecule. To obtain a deeper insight into the nature of the transmission at the Fermi level, the eigenchannel of the Au-C5F-4Py-C-Au molecular junction was calculated at E_{F} (see FIG. 3(d)). A comparison of the

DOI:10.1063/1674-0068/cjcp1911204

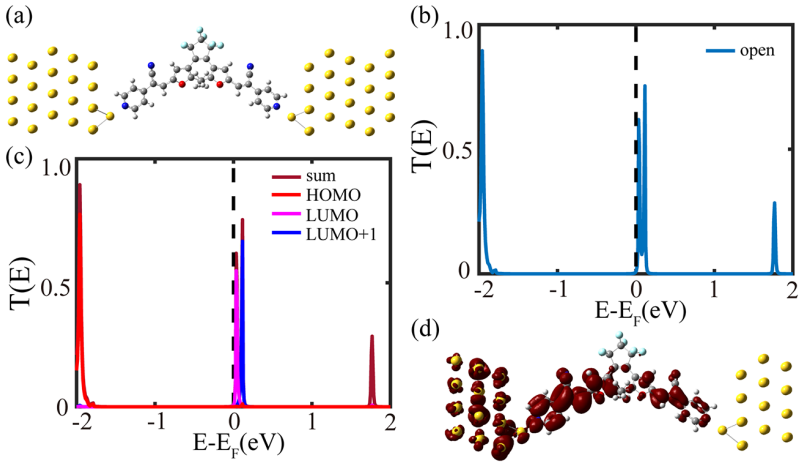

FIG. 3 Optimized atomic structure of the Au-C5F-4Py-C-Au molecular junction (a), equilibrium transmission spectrum of the Au-C5F-4Py-C-Au molecular junction (b), transmission spectrum projected onto the frontier molecular orbitals of isolated C5F-4Py-C molecule (c), and eigenchannel calculated at the Fermi level of the Au-C5F-4Py-C-Au molecular junction (d).

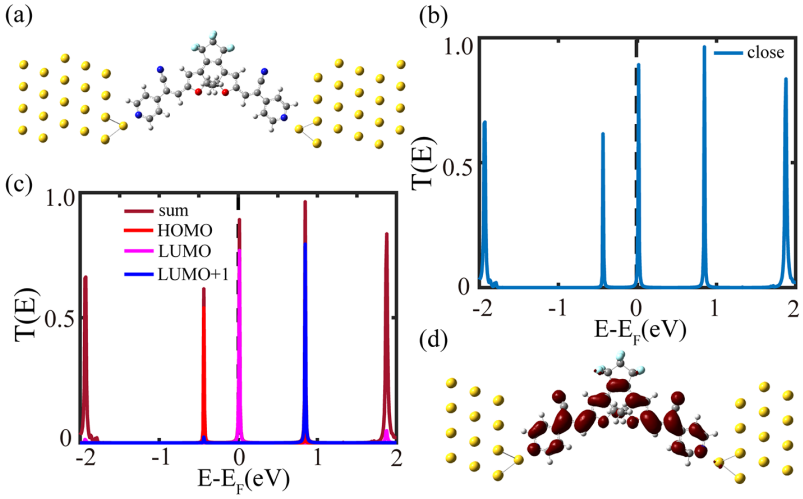

FIG. 4 Optimized atomic structure of Au-C5F-4Py-O-Au molecular junction (a), equilibrium transmission spectrum of the Au-C5F-4Py-O-Au molecular junction (b), transmission spectrum projected onto the frontier molecular orbitals of isolated C5F-4Py-O molecule (c), and eigenchannel calculated at the Fermi level of the Au-C5F-4Py-O-Au molecular junction (d).

eigenchannel state density with the frontier molecular orbitals of the isolated molecule indicated that the electron transport channel at the Fermi level was dominated by the LUMO of the C5F-4Py-C molecule.

The conductance mechanism of the C5F-4Py-C molecular junction has been explained thus far. Although the molecular conformation of C5F-4Py-O will occur when C5F-4Py-C is irradiated by visual light, the transport mechanism of the C5F-4Py-O molecular junction must be investigated further. Hence, we investigated the electronic transport properties of the Au-C5F-4Py-O-Au molecular junction, which was constructed in the same manner as the C5F-4Py-C molecular junction. This was appropriate because the interfacial conformation did not change significantly when it transformed from C5F-4Py-C to C5F-4Py-O or *vice versa*. The optimized distance of the central functional region defined as the C5F-4Py-C molecular junction was 21.79 Å, and the length of the Au−N bond was 2.20 Å, as shown in FIG. 4(a). In addition, the optimized structure of C5F-4Py-O in the molecular junction was similar to that in an isolated situation with comparable bond lengths, bond angles, and dihedral angles. The equilibrium transport spectrum was calculated and is shown in FIG. 4(b). The transmission coefficient at the Fermi level was $6\times10^{-3}\ G_0$. The first transmission peak below the Fermi level was at −1.96 eV. Additionally, the other two prominent transmission peaks were above the Fermi level and were located close to the energy axis. They appeared at 0.035 and 0.12 eV, respectively. By pro-

DOI:10.1063/1674-0068/cjcp1911204

jecting the transmission spectrum onto the molecular orbitals (see FIG. 4(c)), it was discovered that the two peaks were dominated by the LUMO and LUMO+1, respectively. By contrast, the HOMO of C5F-4Py-O contributed to the first transmission peak below the Fermi level. The energy gap acquired from the transmission spectrum was 1.99 eV, which agreed well with that of the isolated C5F-4Py-O molecule. This further confirmed the weak interfacial interaction. At the Fermi level, the contribution to conductance from the LUMO was approximately eight times higher than the contribution of the LUMO+1. Comparing the eigenchannel calculated at the E_{F} (see FIG. 4(d)) of the Au-C5F-4Py-O-Au molecular junction with the orbitals in FIG. 2, we confirmed that the transmission coefficient was mainly ascribed to the LUMO of the C5F-4Py-O molecule. The coupling between Au 5d orbitals and N 2p orbitals contributed to the interfacial interaction. Thus far, we have calculated and interpreted the transport mechanism of the isomers of the C5F-4Py molecule. We discovered that the ratio of the high conductance of C5F-4Py-C to the low conductance of C5F-4Py-O was 41.7, which agreed with the experimental result of 45.9. Although the conductance value calculated in this study was higher than the experimental observation, it did not affect the ratio and mechanism. Considering the similar atomic structure and the same electron transport channel, we inferred that the higher conductance of C5F-4Py-C was ascribed to its LUMO, which was much closer to the Fermi level than that in the case of C5F-4Py-O. In addition, we calculated the electron transfer number between the electrodes and the central molecule in an optimized equilibrium molecular junction. The 0.35 electron transfer to the C5F-4Py-C molecule from the electrodes was higher by 0.23 electrons than that in the C5F-4Py-O molecule. Although the length of the Au−N bond was the same in both isomers, the interfacial interaction between the electrodes and the C5F-4Py-C molecule was much stronger than that in the Au-C5F-4Py-O-Au molecular junction. This may be another reason contributing to the larger conductance value of the Au-C5F-4Py-C-Au molecular junction.

IV. CONCLUSION

In this study, we investigated the atomic and electronic structures of two isomers of C5F-4Py molecules and the electron transfer properties when connecting them to a protruded Au atom along the Au(111) direction using the NEGF+DFT method. Our calculations revealed that the LUMO of the central molecule was critical in determining the low-bias conductance value. Because the atomic structures changed significantly from C5F-4Py-O to C5F-4Py-C, a good electron transport channel was obtained, similar to the alternative single bond and double bond structure of the alkene skeleton crossing the entire C5F-4Py-C molecule, which rendered the electron distribution more delocalized and the conjugation characteristics more remarkable. The greater number of electrons transferred to the C5F-4Py-O molecule from the electrodes in the equilibrium condition caused the LUMO to be nearer to the Fermi energy, which contributed to a large conductance at the Fermi level. Our calculation elucidated the conductive mechanism of the C5F-4Py isomer molecular junctions and the reason for the moderate high-low conductance ratio, which facilitates the design of high-performance molecular switching in the future.

V. ACKNOWLEDGMENTS

This work was supported by the National Natural Science Foundation of China (No.11874242 and No.21933002), the Natural Science Foundation of Shandong Province, China (No.ZR2019PA022).

[1] R. M. Metzger, Chem. Rev. **115**, 5056 (2015).
[2] D. Xiang, X. Wang, C. Jia, T. Lee, and X. Guo, Chem. Rev. **116**, 4318 (2016).
[3] X. Zhang and T. Li, Chin. Chem. Lett. **27**, 1097 (2016).
[4] Z. Liu, S. Ren, and X. Guo, Top. Curr. Chem. **56**, 375 (2016).
[5] T. A. Su, H. Li, R. S. Klausen, N. T. Kim, M. Neupane, J. L. Leighton, M. L. Steigerwald, and L. Venkataraman, Acc. Chem. Res. **50**, 1088 (2017).
[6] R. Frisenda, D. Stefani, and S. J. van der Zant, Acc. Chem. Res. **51**, 1359 (2108).
[7] J. Liu, X. Huang, F. Wang, and W. Hong, Acc. Chem. Res. **52**, 151 (2019).
[8] Y. Miao, S. Qiu, G. Zhang, J. Ren, C. Wang, and G. Hu, Phys. Rev. B **98**, 235415 (2018).
[9] F. Schedin, A. Geim, S. Morozov, E. Hill, P. Blake, M. Katsnelson, and K. Novoselov, Nat. Mater. **6**, 652 (2007).
[10] S. C. Mannsfeld, B. C. Tee, R. M. Stoltenberg, C. V. H-H. Chem, S. Barman, B. V. O. Muir, A. N. Sokolov, C. Reese, and Z. Bao, Nat. Mater. **9**, 859 (2010).
[11] J. D. Re, M. H. Moore, B. R. Ratna, and A. S. Blum, Phys. Chem. Chem. Phys. **15**, 8318 (2013).
[12] C. Zhang, S. Pu, Z. Sun, C. Fan, and G Liu, J. Phys. Chem. B **119**, 4673 (2015).
[13] Z. Li, J. Bi, R. Liu, X. Yi, H. Fu, F. Sun, M. Zhi, and C. Kui, Chin. Phys. B **26**, 098508 (2017).
[14] W. Wu, H. Zhang, Y. Wang, S. Ye, Y. Guo, C. Di, G. Yu, D. Zhu, and Y. Liu, Adv. Funct. Mater. **18**, 2593 (2008).
[15] Y. Wang, J. Kröger, R. Berndt, and W. A. Hofer, J. Am. Chem. Soc. **131**, 3639 (2009).
[16] J. L. Zhang, J. L. Xu, T. C. Niu, Y. H. Lu, L. Liu, and W. Chen, J. Phys. Chem. C **118**, 1712 (2014).
[17] R. Liu, J. Bi, Z. Xie, K. Yin, D. Wang, G. Zhang, D. Xiang, C. Wang, and Z. Li, Phys. Rev. Appl. **9**, 054023 (2018).

DOI:10.1063/1674-0068/cjcp1911204

[18] C. W. Marquardt, S. Grunder, A. Błaszczyk, S. Dehm, F. Hennrich, H. v. Löhneysen, M. Mayor, and R. Krupke, Nat. Nanotechnol. **5**, 863 (2010).
[19] G. Reecht, F. Sheurer, V. Speisser, Y. J. Dappe, F. Mathevet, and G. Schull, Phys. Rev. Lett. **112**, 047403 (2014).
[20] K. Kuhnke, C. Groe, P. Merino, and K. Kern, Chem. Rev. **117**, 5174 (2017).
[21] X. Kong, L. Cai, J. Fan, and L. Lin, Org. Electron. **59**, 7 (2018).
[22] Z. Xie, S. Duan, C. Wang, and Y. Luo, Nanoscale 18189 (2017).
[23] Y. Zhou, X. Wang, C. Tan, and C. Wang, Chin. J. Chem. Phys. **32**, 467 (2019).
[24] H. Song, Y. Kim, Y. H. Jang, H. Jeong, M. A. Reed, and T. Lee, Nature **462**, 1039 (2009).
[25] D. Xiang, H. Jeong, D. Kim, T. Lee, Y. Cheng, Q. Wang, and D. Mayer, Nano Lett. **13**, 2809 (2013).
[26] A. Xiang, H. Li, S. Chen, S. Liu, S. Decurtins, M. Bai, S. Hou, and J. Liao, Nanoscale **7**, 7665 (2015).
[27] H. Sun, X. Liu, Y. Su, B. Deng, H. Peng, S. Decurtins, S. Sanvito, S. Liu, S. Hou, and J. Liao, Nanoscale **11**, 13117 (2019).
[28] H. Wan, B. Zhou, X. Chen, C. Q. Sun, and G. Zhou, J. Phys. Chem. C **116**, 2570 (2012).
[29] H. Wan, Y. Xu, and G. Zhou, J. Chem. Phys. **136**, 184704 (2012).
[30] C. Jian, L. Cao, X. Zhou, B. Zhou, and G. Zhou, J. Phys.: Condens. Matter **30**, 265301 (2018).
[31] C. Jia, A. Migliore, N. Xin, S. Huang, J. Wang, Q. Yang, S. Wang, H. Chen, D. Wang, B. Feng, Z. Liu, G. Zhang, D. Qu, H. Tian, M. A. Ratner, H. Q. Xu, A. Nitzan, and X. Guo, Science **352**, 1443 (2016).
[32] G. Zhang, Y. Mu, J. Zhao, H. Huang, G. Hu, Z. Li, and C. Wang, Physica E **109**, 1 (2019).
[33] Y. Meng and T. Liu, Acc. Chem. Res. **52**, 1369 (2019).
[34] Z. Xie, S. Duan, G. Tian, C. Wang, and Y. Luo, Nanoscale **10**, 11850 (2018).
[35] L. Cai, M. A. Cabass, H. Yoon, O. M. Cabarcos, C. L. McGuiness, A. K. Flatt, D. L. Allara, J. M. Tour, and T. S. Mayer, Nano Lett. **5**, 2365 (2005).
[36] B. Choi, S. Kahng, S. Kim, H. Kim, H. W. Kim, Y. J. Song, J. Ihm, and Y. Kuk, Phys. Rev. Lett. **96**, 156106 (2006).
[37] P. Liljeroth, J. Repp, and G. Meyer, Science **317**, 1203 (2007).
[38] M. Alemani, M. V. Peters, S. Hecht, K. Rieder, F. Moresco, and L. Grill, J. Am. Chem. Soc. **128**, 14446 (2006).
[39] J. Wirth, N. Hatter, R. Drost, T. R. Umbach, S. Barja, M. Zastrow, K. Rck-Braun, J. I. Pascual, P. Saalfrank, and K. J. Franke, J. Phys. Chem. C **119**, 4874 (2015).
[40] A. Khodko, V. Khomenko, Y. Shynkarenko, O. Mamuta, O. Kapitanchuk, D. Sysoiev, N. Kachalova, T. Huhn, and S. Snegir, Chem. Phys. Lett. **669**, 156 (2017).
[41] A. Khodko, N. Kachalova, S. Scherbakov, A. Eremenko, and L. Mukha, Nanoscale Res. Lett. **12**, 271 (2017).
[42] F. Nickel, M. Bernien, M. Herder, S. Wrzalek, P. Chittas, K. Kraffert, L. M. Arruda, L. Kipgen, D. Krger, S. Hecht, and W. Kuch, J. Phys.: Condens. Matter **29**, 374001 (2017).
[43] Y. Kurokawa, R. Hayakawa, S. Shimada, K. Higashiguchi, Y. Noguchi, K. Matsuda, and Y. Wakayama, Org. Electron. **64**, 205 (2019).
[44] M. Irie, Y. Yokoyama, and T. Seki, *New Frontiers in Photochromism*, Japan: Springer, (2013).
[45] K. Uchida, Y. Yamanoi, T. Yonezawa, and H. Nishihara, J. Am. Chem. Soc. **133**, 9239 (2011).
[46] M Irie, T. Fukaminato, K. Matsuda, and S. Kobatake, Chem. Rev. **114**, 12174 (2014).
[47] D. Dulić, S. J. van der Molen, T. Kudernac, H. T. Jonkman, J. J. D. de Jong, T. N. Bowden, J. van Esch, B. L. Feringa, and B. J. van Wees, Phys. Rev. Lett. **91**, 207402 (2003).
[48] Y. Kim, T. J. Hellmuth, D. Sysoiev, F. Pauly, T. Pietsch, J. Wolf, A. Erbe, T. Huhn, U. Groth, U. E. Steiner, and E. Scheer, Nano Lett. **12**, 3736 (2012).
[49] C. Jia, J. Wang, C. Yao, Y Cao, Y Zhong, Z. Liu, Z. Liu, and X. Guo, Angew. Chem. Int. Ed. **52**, 8666 (2013).
[50] G. Reecht, C. Lotze, D. Sysoiev, T. Huhn, and K. J. Franke, ACS Nano **10**, 10555 (2016).
[51] G. Reecht, C. Lotze, D. Sysoiev, T. Huhn, and K. J. Franke, J. Phys.: Condens. Matter **29**, 294001 (2017).
[52] Y. Meir and N. S. Wingreen, Phys. Rev. Lett. **68**, 2512 (1992).
[53] P. Hohenberg and W. Kohn, Phys, Rev. **136**, B864 (1964).
[54] Y. Xue, S. Datta, and M. A. Ratner, Chem. Phys. **281**, 151 (2002).
[55] M. Brandbyge, J. Mozos, P. Ordejón, J. Taylor, and K. Stokbro, Phys. Rev. B **65**, 165401 (2002).
[56] R. Li, J. Zhang, Z. Qian, Z. Shen, X. Zhao, and Z. Xue, Chem. Phys. **336**, 127 (2007).
[57] A. R. Rocha, V. M. García-Suárez, S. W. Bailey, C. J. Lambert, J. Ferrer, and S. Sanvito, Nat. Mater. **4**, 335 (2005).
[58] N. Troullier and J. L. Martins, Phys. Rev. B **43**, 1993 (1991).
[59] J. M. Soler, E. Artacho, J. D. Gale, A. García, J. Junquera, P. Ordejón, and D. Sánchez-Portal, J. Phys.: Condens Matter **14**, 2745 (2002).
[60] J. P. Perdew, K. Burke, and M. Ernzerhof, Phys. Rev. Lett. **77**, 3865 (1996).
[61] J. Zhang and H. Tian, Adv. Optical Mater. **6**, 1701278 (2018).
[62] T. Fukaminato and M. Irie, *Diarylethenes that Photoswitch with Visible Light*, Y. Yokoyama and K. Nakatani Eds., Tokyo: Photon-Working Switches, Springer, (2017).
[63] L. Han, X. Zuo, H. Li, Y. Li, C. Fang, and D. Liu, J. Phys. Chem. C **123**, 2736 (2019).

DOI:10.1063/1674-0068/cjcp1911204